Supplemental Material for "Mechanism of screening or enhancing the pseudogap throughout the two-band Bardeen-Cooper-Schrieffer to Bose-Einstein condensate crossover"

Hiroyuki Tajima,[1,2] Yuriy Yerin,[3,4] Pierbiagio Pieri,[5,6] and Andrea Perali[7]

[1]*Department of Mathematics and Physics, Kochi University, Kochi 780-8520, Japan*
[2]*RIKEN Nishina Center, Wako, Saitama, 351-0198, Japan*
[3]*Dipartimento di Fisica e Geologia, Università di Perugia, I-06123 Perugia, Italy*
[4]*School of Science and Technology, Physics Division, Università di Camerino, 62032 Camerino (MC), Italy*
[5]*Dipartimento di Fisica e Astronomia, Università di Bologna, I-40127 Bologna, Italy*
[6]*INFN, Sezione di Bologna, I-40127 Bologna, Italy*
[7]*School of Pharmacy, Physics Unit, Università di Camerino, 62032 Camerino (MC), Italy*

(Dated: November 19, 2020)

PACS numbers: 03.75.Ss, 74.20.-z, 74.25.-q

I. ANALYTIC CONTINUATION WITH THE PADÉ APPROXIMANTS

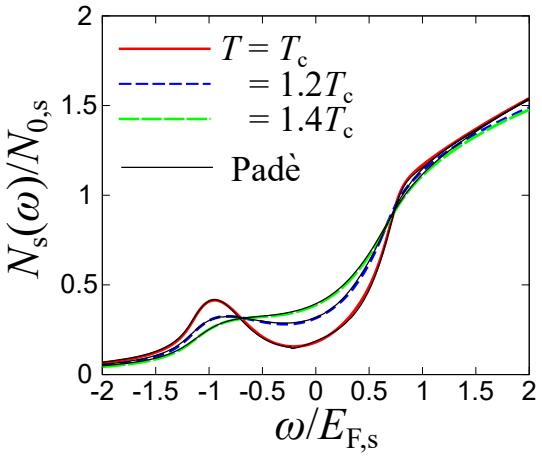

FIG. 1: Comparison of the DOS $N_s(\omega)$ in the single-band system at $T = T_c$, $1.2T_c$, and $1.4T_c$ obtained from the exact analytical continuation from Ref. [1] as well as the Padé approximants (thin curves). The parameters are set at $(k_F a)^{-1} = 0$. $N_{s,0} = m\sqrt{2mE_{F,s}}/(2\pi^2)$ is the DOS at the Fermi level for a non-interacting Fermi gas at $T = 0$.

In this Supplemental Material, we show the validity of the Padé approximants, which assume that $\Sigma_i(\boldsymbol{p}, z)$ with the complex frequency argument z for given $\boldsymbol{p}$ is in the form

$$\Sigma_i(\boldsymbol{p}, z) = \frac{\alpha_1 + \alpha_2 z + \cdots + \alpha_j z^{j-1}}{\beta_1 + \beta_2 z + \cdots + \beta_j z^{j-1} + z^j}. \tag{1}$$

The parameters $\{\alpha_k, \beta_k\}$ $(k = 1, \cdots, j)$ are determined by the $2j$ numerical values of $\Sigma_i(\boldsymbol{p}, i\omega_\ell)$ along the imaginary axis. In this work, we use 200 $(= 2j)$ data.

In the T-matrix approach, one can analytically perform the analytic continuation [1]. The imaginary part of the retarded self-energy in this approximation can be written as

$$\mathrm{Im}\Sigma_i(\boldsymbol{k}, \omega) = -\sum_{\boldsymbol{q}} \mathrm{Im}\Gamma_{ii}(\boldsymbol{q}, \omega + \xi_{\boldsymbol{q}-\boldsymbol{k},i}) \left[b(\omega + \xi_{\boldsymbol{q}-\boldsymbol{k},i}) + f(\xi_{\boldsymbol{q}-\boldsymbol{k},i})\right], \tag{2}$$

where $b(x) = [e^{x/T} - 1]^{-1}$ and $f(x) = [e^{x/T} + 1]^{-1}$ are Bose and Fermi distribution functions, respectively. The real part of the self-energy can be obtained via the Kramers-Kronig relation

$$\mathrm{Re}\Sigma_i(\boldsymbol{k}, \omega) = \frac{1}{\pi}\mathcal{P}\int_{-\infty}^{\infty} d\omega' \frac{\mathrm{Im}\Sigma_i(\boldsymbol{k}, \omega)}{\omega' - \omega}, \tag{3}$$

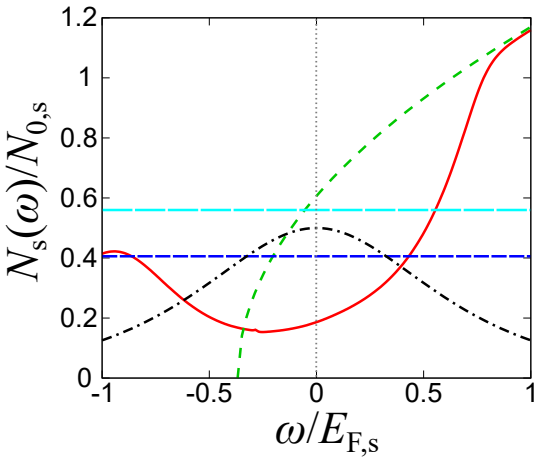

FIG. 2: Comparison of the DOS $N_s(\omega)$ obtained from the Padé approximants (solid curve) and $-G_s(\boldsymbol{r}=\boldsymbol{0},\tau=\beta/2)\beta/\pi = 0.405N_{0,s}$ (dashed line) in the single-band model at $T=T_c=0.243T_{F,s}$ in the unitarity limit. We also plot the square-root type DOS in a non-interacting counterpart and $-G_s^0(\boldsymbol{r}=\boldsymbol{0},\tau=\beta/2)\beta/\pi = 0.560N_{0,s}$ (long-dashed line). The dash-dotted curve shows the weight factor $1/\left[2\cosh(\beta\omega/2)\right]$ in Eq. (5).

where $\mathcal{P}$ is the Cauchy principal value. To see how the Padé approximants work in the analytic continuation procedure, we compare the DOS with the exact analytic continuation in Ref. [1] and that with the Padé approximants in the T-matrix approach. For simplicity, we consider the single-band system ($i=\mathrm{s}$). Here we define the non-interacting DOS at the Fermi level $N_{0,s}=\frac{m\sqrt{2mE_{F,s}}}{2\pi^2}$ where $E_{F,s}$ is the Fermi energy at $T=0$ in the single-band system. Figure 1 shows the DOS at unitarity in the single-band system at $T=T_c$, $1.2T_c$, and $1.4T_c$. The results with the Padé approximants represented by the thin curves show an excellent agreement with those with exact analytic continuation done in Ref. [1] even near $T=T_c$.

For comparison, we calculate the single-particle Green's function $G_i(\boldsymbol{r},\tau)$ with the spatial position $\boldsymbol{r}$ and the imaginary time τ, which is given by

$$G_i(\boldsymbol{r},\tau)=T\sum_{\boldsymbol{k},i\omega_l} G_i(\boldsymbol{k},i\omega_l)e^{i(\boldsymbol{k}\cdot\boldsymbol{r}-\omega_l\tau)}. \tag{4}$$

At sufficiently low temperature, it is related to $N_i(\omega=0)$ as [2]

$$\begin{aligned} G_i(\boldsymbol{r}=0,\tau=\beta/2) &= -\frac{1}{2}\int_{-\infty}^{\infty}d\omega\frac{N_i(\omega)}{\cosh(\beta\omega/2)} \\ &= -\frac{1}{2}N_i(0)\int_{-\infty}^{\infty}\frac{d\omega}{\cosh(\beta\omega/2)}\left[1+\frac{\omega}{N_i(0)}\left.\frac{dN_i(\omega)}{d\omega}\right|_{\omega=0}+\cdots\right] \\ &\simeq -\frac{\pi}{\beta}N_i(\omega=0), \end{aligned} \tag{5}$$

where $\beta=1/T$ is the inverse temperature. The correction originating from the leading-order term is proportional to T^2, which is neglected for simplicity. We evaluate $G_i(\boldsymbol{r}=\boldsymbol{0},\tau=\beta/2)$ as

$$\begin{aligned} G_i(\boldsymbol{r}=\boldsymbol{0},\tau) &= \sum_{\boldsymbol{k}} e^{-\xi_{\boldsymbol{k},i}\tau}\left[f(\xi_{\boldsymbol{k},i})-1\right] \\ &\quad +T\sum_{\boldsymbol{k},i\omega_l}\left[G_i(\boldsymbol{k},i\omega_l)-G_i^0(\boldsymbol{k},i\omega_l)\right]e^{-i\omega_l\tau}, \end{aligned} \tag{6}$$

where the Matsubara frequency sum is evaluated numerically (see Sec. II).

First, we consider the single-band case. Figure 2 shows the comparison between $N_s(\omega)$ and $G_s(\boldsymbol{r}=\boldsymbol{0},\tau=\beta/2)\beta/\pi$ where G_s is the single-particle Green's function in the single-band Fermi gas. In a non-interacting case with same μ and T, we obtain $G_s^0(\boldsymbol{r}=\boldsymbol{0},\tau=\beta/2)\beta/\pi=0.560N_{0,s}$, which is close to $N_{0,s}(\omega=0)=m\sqrt{2m\mu_s}/2\pi^2\simeq 0.606N_{0,s}$ where μ_s is the single-band chemical potential. The difference between them originates from the leading-order correction in Eq. (5). In the strongly interacting case, we obtain $G_s(\boldsymbol{r}=\boldsymbol{0},\tau=\beta/2)\beta/\pi\simeq 0.405N_{0,s}$. Although it is smaller than

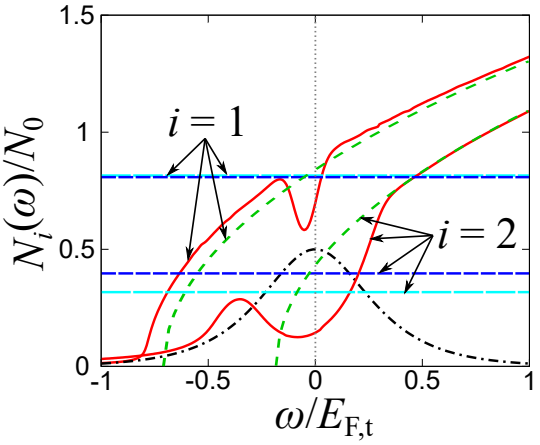

FIG. 3: Same plots with Fig. 2 in a two-band Fermi gas. The parameters are $T = T_{\rm c} = 0.113T_{\rm F,t}$, $(k_{\rm F,1}a_{11})^{-1} = -2$, $(k_{\rm F,2}a_{22})^{-1} = -0.6$, and $\lambda_{12} = 2$. The weight factor $1/[2\cosh(\beta\omega/2)]$ (dash-dotted curve) in Eq. (5) is also plotted.

the non-interacting counterpart, it is larger than the result with the analytic continuation with the Padé approximants given by $N_{\rm s}(\omega = 0) = 0.186N_{0,{\rm s}}$. This is also expected to be the leading-order corrections in Eq. (5), which involve not only $N_{\rm s}(\omega = 0)$ but also $N_{\rm s}(\omega \neq 0)$ multiplied by the weight factor $1/[2\cosh(\beta\omega/2)]$ shown in Fig. 2. To see this, we evaluate the same quantity using $N_{\rm s}(\omega)$ obtained from the analytic continuation with the Padé approximants, resulting in $G_{\rm s}(\boldsymbol{r} = \boldsymbol{0}, \tau = \beta/2)\beta/\pi \simeq 0.408N_{0,{\rm s}}$ Indeed, it is close to that obtained from Eq. (6) with the Matsubara Green's function $G_{\rm s}(\boldsymbol{k}, i\omega_l)$.

Figure 3 shows the comparison between $N_i(\omega)$ obtained by the analytic continuation with the Padé approximants and $-G_i(\boldsymbol{r} = \boldsymbol{0}, \tau = \beta/2)\beta/\pi$ in a strongly interacting two-band Fermi gas with $(k_{\rm F,1}a_{11})^{-1} = -2$, $(k_{\rm F,2}a_{22})^{-1} = -0.6$, and $\lambda_{12} = 2$ at $T = T_{\rm c}$. In the weakly-interacting deep band ($i = 1$), we obtain $-G_1(\boldsymbol{r} = \boldsymbol{0}, \tau = \beta/2)\beta/\pi \simeq 0.815N_0$ which is close to the non-interacting counterpart given by $0.808N_0$ due to the cancellation of two contributions, that is, the pseudogap suppression and the band-renormalization enhancement of the DOS. In the strongly-interacting shallow band, we obtain $-G_2(\boldsymbol{r} = \boldsymbol{0}, \tau = \beta/2)\beta/\pi \simeq 0.317N_0$ which is smaller than the non-interacting counterpart given by $0.397N_0$. However, it is larger than the results of Padé approximants given by $N_2(\omega = 0) = 0.144N_0$ due to the contribution from $N_2(\omega \neq 0)$.

II. MATSUBARA FREQUENCY SUM

We evaluate numerically the Matsubara frequency sum in the self-energy $\Sigma_i(\boldsymbol{p}, i\omega_l)$ as

$$\Sigma_i(\boldsymbol{p}, i\omega_l) \;=\; U_{ii}n_i^0 + T\sum_{\boldsymbol{p}}\sum_{\ell}^{|\ell|\le n_{\rm cut,b}} \left[\Gamma_{ii}(\boldsymbol{q}, i\nu_\ell) - U_{ii}\right] G_i^0(\boldsymbol{q}-\boldsymbol{p}, i\nu_\ell - i\omega_l), \tag{7}$$

where n_i^0 is the number density for a non-interacting gas and we introduce the cutoff number $n_{\rm cut,b}$. We take $n_{\rm cut,b} = 1000 \sim 50000$, depending on the coupling parameters as well as the temperature. In addition, we add the contribution beyond $n_{\rm cut,b}$ by approximately transforming the summation into continuous integration [3]. In Fig. 4, we show the dependence by $n_{\rm cut,b}$ of the typical self-energy $\Sigma_i(\boldsymbol{p} = \boldsymbol{0}, i\omega_l = i\pi T)$ at $T = T_{\rm c}$ with $(k_{\rm F,1}a_{11})^{-1} = -2$, $(k_{\rm F,2}a_{22})^{-1} = 0$, and $\lambda_{12} = 1$. We find sufficient convergences of them within the relative errors of 0.01% in both bands.

We note that the Matsubara frequency sum in $\Pi_{\ell\ell}(\boldsymbol{q}, i\nu_l)$ can analytically be performed as

$$\Pi_{\ell\ell}(\boldsymbol{q}, i\nu_l) = \sum_{\boldsymbol{p}} \frac{1 - f(\xi_{\boldsymbol{p}+\boldsymbol{q},\ell}) - f(\xi_{\boldsymbol{p},\ell})}{i\nu_l - \xi_{\boldsymbol{p}+\boldsymbol{q},\ell} - \xi_{\boldsymbol{p},\ell}}. \tag{8}$$

In the case of the number density n_i, we decompose the equation with the non-interacting density n_i^0, the NSR correction $\delta n_i^{\rm NSR}$ [4], and the remaining part δn_i as

$$n_i \;=\; 2\sum_{\boldsymbol{k}} f(\xi_{\boldsymbol{k},i}) + 2T\sum_{\boldsymbol{k},i\omega_n} \left\{G_i^0(\boldsymbol{k}, i\omega_n)\right\}^2 \Sigma_i(\boldsymbol{k}, i\omega_n)$$

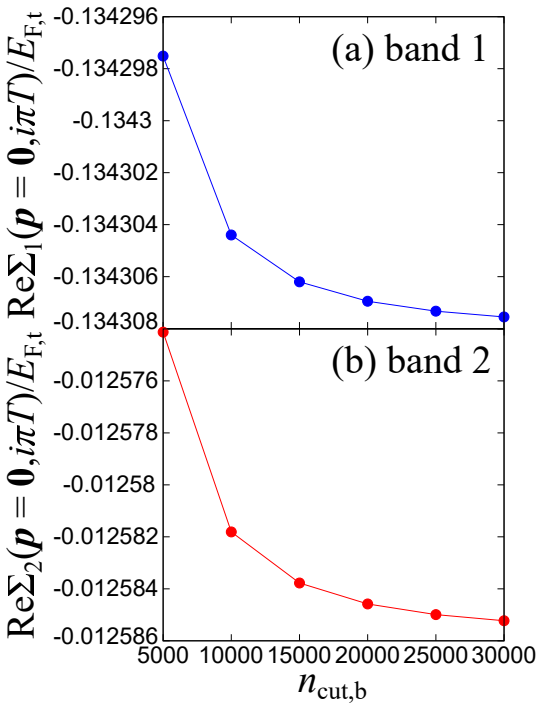

FIG. 4: The real part of the self-energies $\mathrm{Re}\Sigma_i(\boldsymbol{p}=\boldsymbol{0},i\omega_l=i\pi T)$ in (a) the deep band ($i=1$) and the shallow band ($i=2$) as a function of the bosonic Matsubara frequency cutoff $n_{\mathrm{cut,b}}$ in a two-band Fermi gas at $T=T_{\mathrm{c}}$ with $(k_{\mathrm{F},1}a_{11})^{-1}=-2$, $(k_{\mathrm{F},2}a_{22})^{-1}=0$, and $\lambda_{12}=1$.

$$
\begin{aligned}
&+2T\sum_{\boldsymbol{k},i\omega_n}\left[G_i(\boldsymbol{k},i\omega_n)-G_i^0(\boldsymbol{k},i\omega_n)-\left\{G_i^0(\boldsymbol{k},i\omega_n)\right\}^2\Sigma_i(\boldsymbol{k},i\omega_n)\right]\\
\equiv\ & n_i^0+\delta n_{\mathrm{NSR}}+\delta n_i. \qquad (9)
\end{aligned}
$$

Using the same technique in Eq. (8), we can analytically perform the fermionic Matsubara summation in $\delta n_i^{\mathrm{NSR}}$ as [4]

$$
\delta n_i^{\mathrm{NSR}}=-T\sum_{\boldsymbol{q},i\nu_l}\frac{U_{ii}[1+U_{\bar{i}\bar{i}}\Pi_{\bar{i}\bar{i}}(\boldsymbol{q},i\nu_l)]-U_{12}U_{21}\Pi_{\bar{i}\bar{i}}(\boldsymbol{q},i\nu_l)}{[1+U_{11}\Pi_{11}(\boldsymbol{q},i\nu_l)][1+U_{22}\Pi_{22}(\boldsymbol{q},i\nu_l)]-U_{12}U_{22}\Pi_{11}(\boldsymbol{q},i\nu_l)\Pi_{22}(\boldsymbol{q},i\nu_l)}\frac{\partial\Pi_{ii}(\boldsymbol{q},i\nu_l)}{\partial\mu}, \qquad (10)
$$

where $\bar{i}$ denotes the opposite band index of i (e.g. $\bar{i}=1$ when $i=2$). We note that the bosonic Matsubara frequency sum in Eq. (10) is numerically evaluated with the same technique used for the self-energy calculation in Eq. (7).

When we perform the fermionic Matsubara sum in δn_i, we introduce the cutoff number $n_{\mathrm{cut,f}}$ as

$$
\delta n_i=2T\sum_{\boldsymbol{p}}\sum_{n}^{|n|\le n_{\mathrm{cut,f}}}\left[G_i(\boldsymbol{k},i\omega_n)-G_i^0(\boldsymbol{k},i\omega_n)-\left\{G_i^0(\boldsymbol{k},i\omega_n)\right\}^2\Sigma_i(\boldsymbol{k},i\omega_n)\right], \qquad (11)
$$

in which the convergence with respect to $n_{\mathrm{cut,f}}$ is faster compared to the summation of $G_i(\boldsymbol{k},i\omega_n)$ without the decomposition. Figure 5 shows the $n_{\mathrm{cut,f}}$ dependence of δn_i in a two-band Fermi gas at $T=T_{\mathrm{c}}$ with $(k_{\mathrm{F},1}a_{11})^{-1}=-2$, $(k_{\mathrm{F},2}a_{22})^{-1}=0$, and $\lambda_{12}=1$. We find sufficient convergences for $n_{\mathrm{cut,f}}$ at each coupling parameter and temperature. We use $n_{\mathrm{cut,f}}=200\sim300$, checking their convergences within the relative errors of 0.01%.

[1] F. Palestini, A. Perali, P. Pieri, and G. C. Strinati, *Dispersions, weights, and widths of the single-particle spectral function in the normal phase of a Fermi gas*, Phys. Rev. B **85**, 024517 (2012).

[2] N. Trivedi and M. Randeria, *Deviations from Fermi-Liquid Behavior above T_{c} in 2D Short Coherence Length Superconductors*, Phys. Rev. Lett. **75**, 312 (1995).

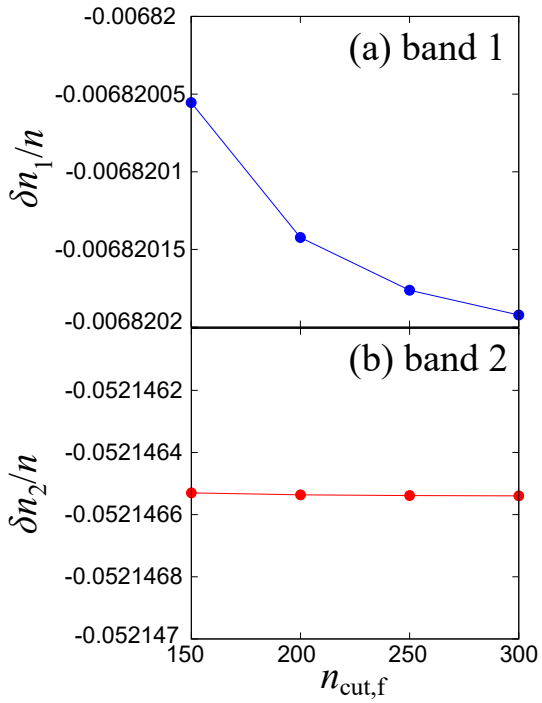

FIG. 5: The correction beyond the NSR approach to the number densities (a)δn_1 and (b)δn_2 as a function of the fermionic Matsubara frequency cutoff $n_{\mathrm{cut,b}}$ in a two-band Fermi gas at $T = T_{\mathrm{c}}$ with $(k_{\mathrm{F},1}a_{11})^{-1} = -2$, $(k_{\mathrm{F},2}a_{22})^{-1} = 0$, and $\lambda_{12} = 1$.

[3] P. Pieri, L. Pisani, and G. C. Strinati, *BCS-BEC crossover at finite temperature in the broken symmetry phase*, Phys. Rev. B **70**. 094508 (2004).
[4] H. Tajima, A. Perali, and P. Pieri, *BCS-BEC Crossver and Pairing Fluctuations in a Two-Band Superfluid/Superconductor: A T Matrix Approach*, Condens. Matter **5**, 10 (2020).